Nature-inspired hierarchical building materials with low CO_2 emission and superior performance

Jinyang Jiang[1], Han Wang[1], Junlin Lin[1], Fengjuan Wang[1], Zhiyong Liu[1], Liguo Wang[1], Zongjin Li[2], Yali Li[3], Yunjian Li [2] ✉ & Zeyu Lu [1] ✉
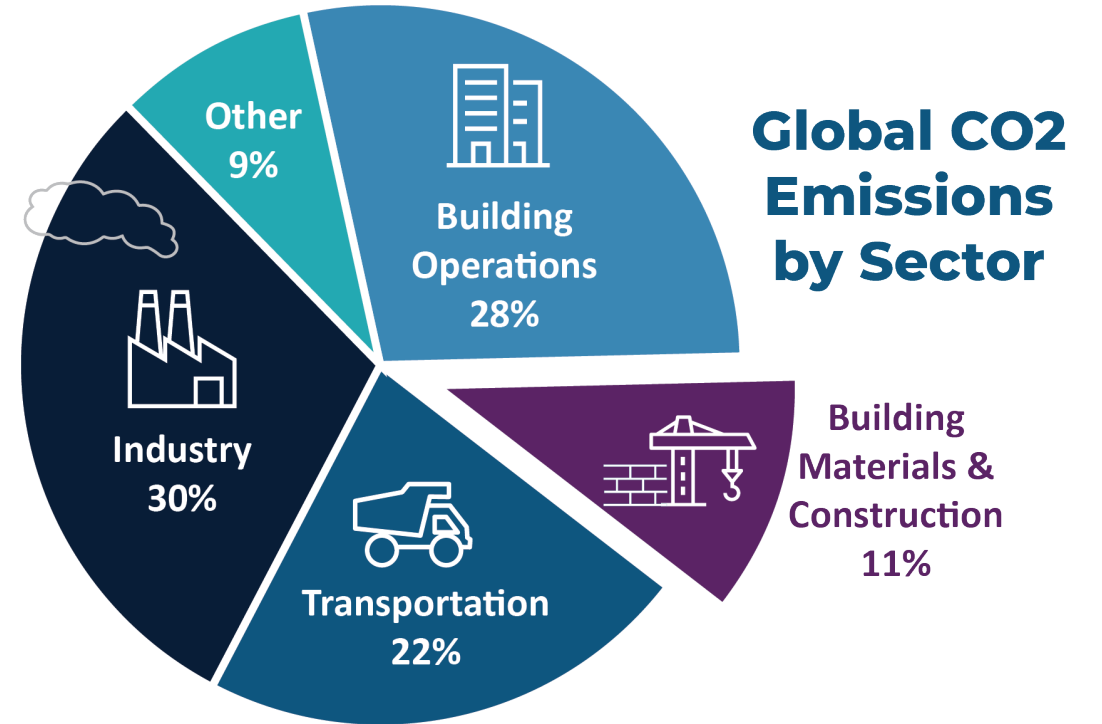
a. Jiangsu Key Laboratory of Construction Materials, School of Materials Science and Engineering, Southeast University, Nanjing 211189, China;

b. Centre for Smart Infrastructure and Digital Construction, School of Engineering, Swinburne University of Technology, Hawthorn, Victoria, 3122 Australia.

c. Faculty of Innovation Engineering, Macau University of Science and Technology, Macau SAR, 999078, China

Presented by

Riya Dutta

26-04-2025

Introduction

Global CO2 Emissions by Sector

- Other 9%
- Building Operations 28%
- Industry 30%
- Transportation 22%
- Building Materials & Construction 11%

Source: Adapted from the World Green Building Council, Global Status report, 2019.

Decarbonization of the cement sector

1. Clinker substitution with SCMs (recycled solid waste materials)

Cement and Concrete Research
Volume 114, December 2018, Pages 2-26

ELSEVIER

Cement and Concrete Research

Eco-efficient cements: Potential economically viable solutions for a low-CO_2 cement-based materials industry ☆

UN Environment, Karen L. Scrivener [a], Vanderley M. John [b], Ellis M. Gartner [c]

2. Electrochemical process to produce and recycle cement with zero or negative carbon emissions

Energy & Environmental Science

ROYAL SOCIETY OF CHEMISTRY

PAPER

View Article Online
View Journal | View Issue

Check for updates

Scalable electrified cementitious materials production and recycling†

Cite this: Energy Environ. Sci., 2024, 17, 9566

Xiao Kun Lu, [‡ab] Wenxin Zhang,[‡ac] Brianna N. Ruggiero,[b] Linsey C. Seitz [*b] and Jiaqi Li [*ad]

4. Conversion of CO_2 into other useful product

ACS Sustainable Chemistry & Engineering > Vol 10/Issue 1 > Article

Open Access

Cite   Share

RESEARCH ARTICLE | December 11, 2021

Deep Decarbonization of the Cement Sector: A Prospective Environmental Assessment of CO_2 Recycling to Methanol

Marta Rumayor*, Javier Fernández-González, Antonio Domínguez-Ramos, and Angel Irabien

3. Carbon capture, utilization, and storage (CCUS)

ACS Sustainable Chemistry & Engineering

pubs.acs.org/journal/ascecg

This article is licensed under CC-BY 4.0

Research Article

Integrated Carbon Capture and Utilization in the Cement Industry: A Comparative Study

Mattheus Meijssen, Viola Becattini, and Marco Mazzotti*

Lightweight cement/concrete

Benefits of light weight concrete	Impact on Carbon Emissions
Lower density	Less material and cement required per volume
Easier handling/transport	Reduced energy use in logistics
Incorporation of byproducts	Less reliance on high-carbon cement
Improved durability	Fewer repairs and replacements needed

Lightweight cement/concrete

Review

Physical and functional characteristics of foam concrete: A review

Amritha Raj, Dhanya Sathyan, K.M. Mini

ADVANCED SCIENCE

Wood-Inspired Cement with High Strength and Multifunctionality

Faheng Wang, Yuanbo Du, Da Jiao, Jian Zhang, Yuan Zhang, Zengqian Liu

Foam technology

- Large amounts of **macropores** thus lower the density (2.2-2.4 g/cm^3 to 0.01-1.2g/cm^3).
- The stress concentration caused by large pores leads to a significant **sacrifice of mechanical performance** (compressive strength: 0.2-10 MPa, flexural strength: 0.05-4 MPa)
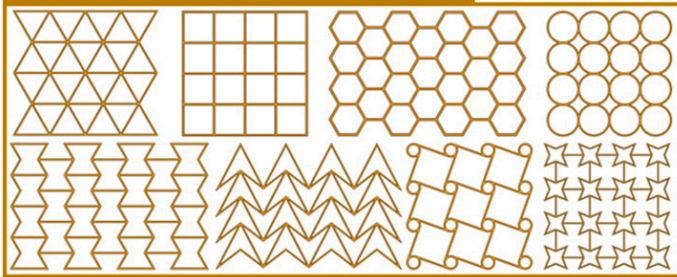
Ice-template technique

- **Smaller pore** sizes ranging from 10-500 µm.
- The regularly arranged smaller pores contribute to much **improved compressive strength** (20-50 MPa) and **toughness** (10-14 MJ·m^{-3}) along the direction of ice crystal growth
- But owing to the **anisotropic nature** of materials a 300%-500% reduction in mechanical strength in the transverse direction.
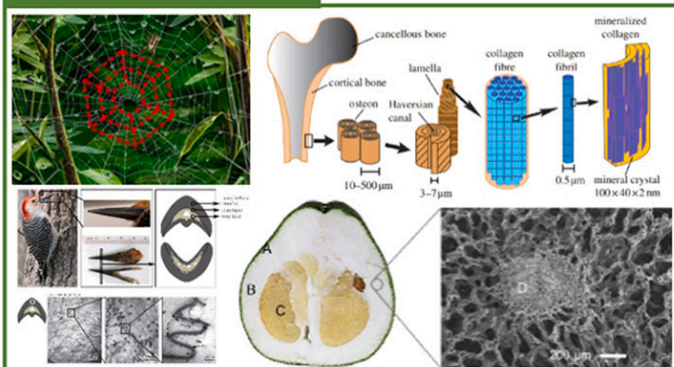
Advanced honeycomb designs for improving mechanical properties: A review

Chang Qi [a b], Feng Jiang [a], Shu Yang [a c]
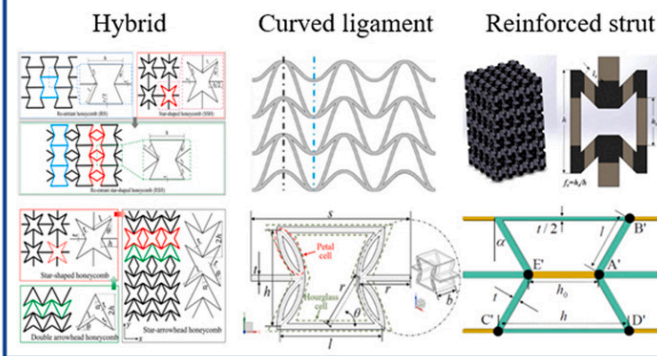
The controlled design on the shape and size of micro- and nano-pores in cement-based materials has not been previously investigated within the relevant field.

Classic honeycomb configurations

Biomimetic structures

Advanced designs

Macro-scale
Hierarchical   Graded   Disordered

Meso-scale
Hybrid   Curved ligament   Reinforced strut

Compared with normal cement paste, LLST exhibited

- 54% reduction in density
- 49% reduction in carbon emissions
- 145% improvement in specific compressive strength
- 1460% improvement in fracture energy
- a more convenient fabrication process in 10 min
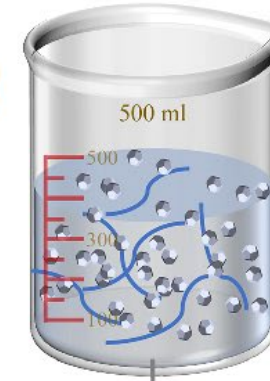- 20% higher utilization rate of raw materials

The fabrication process of LLST

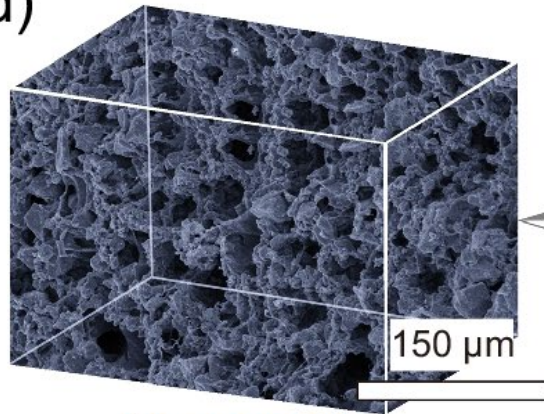(a) Solution of hydrogel monomer

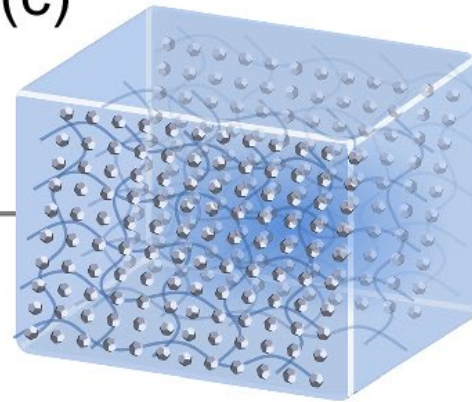(NIPAm) (SA) (Bis) (APS)
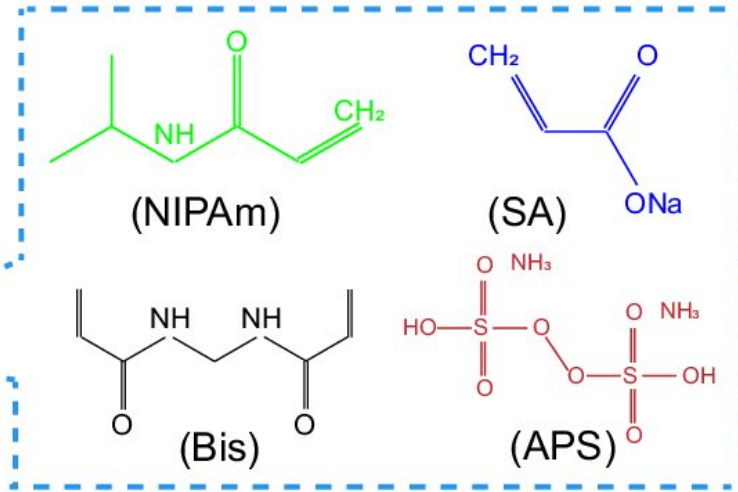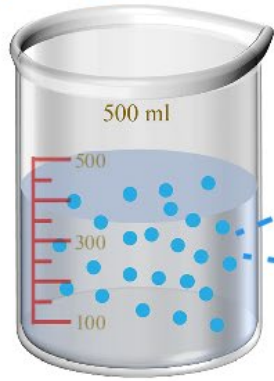
(b) Addition of cement

1. NIPAm: N-isopropylacrylamide
2. SA: Sodium acrylate
3. Bis: N,N-methylenebisacrylamide
4. APS: Potassium persulfate
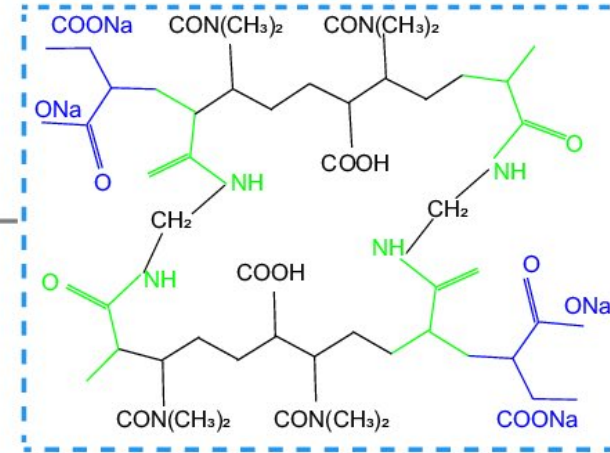5. TEMED: N,N,N',N'-tetramethylethylenediamine

(c) Cement deposition and in situ hydration

Rapid gelation

(d) Sponge-like porous structure

150 µm

Table 1 | Mix designs of different LLST

Mix. (g)	LLST-1	LLST-2	LLST-3	LLST-4	Reference (Ref.)	NIPAm-SA
Cement	20	40	60	80	80	–
Water	40	40	40	40	40	40
NIPAm	3.2	3.2	3.2	3.2	–	3.2
SA	0.8	0.8	0.8	0.8	–	0.8
Bis	0.06	0.06	0.06	0.06	–	0.06
APS	0.06	0.06	0.06	0.06	–	0.06
TEMED (µL)	60	60	60	60	–	60
Water-to-cement	2	1	0.67	0.5	0.5	

Curing: The mixture was placed in a curing container with a temperature of 20 ºC and RH of 95% until tested.
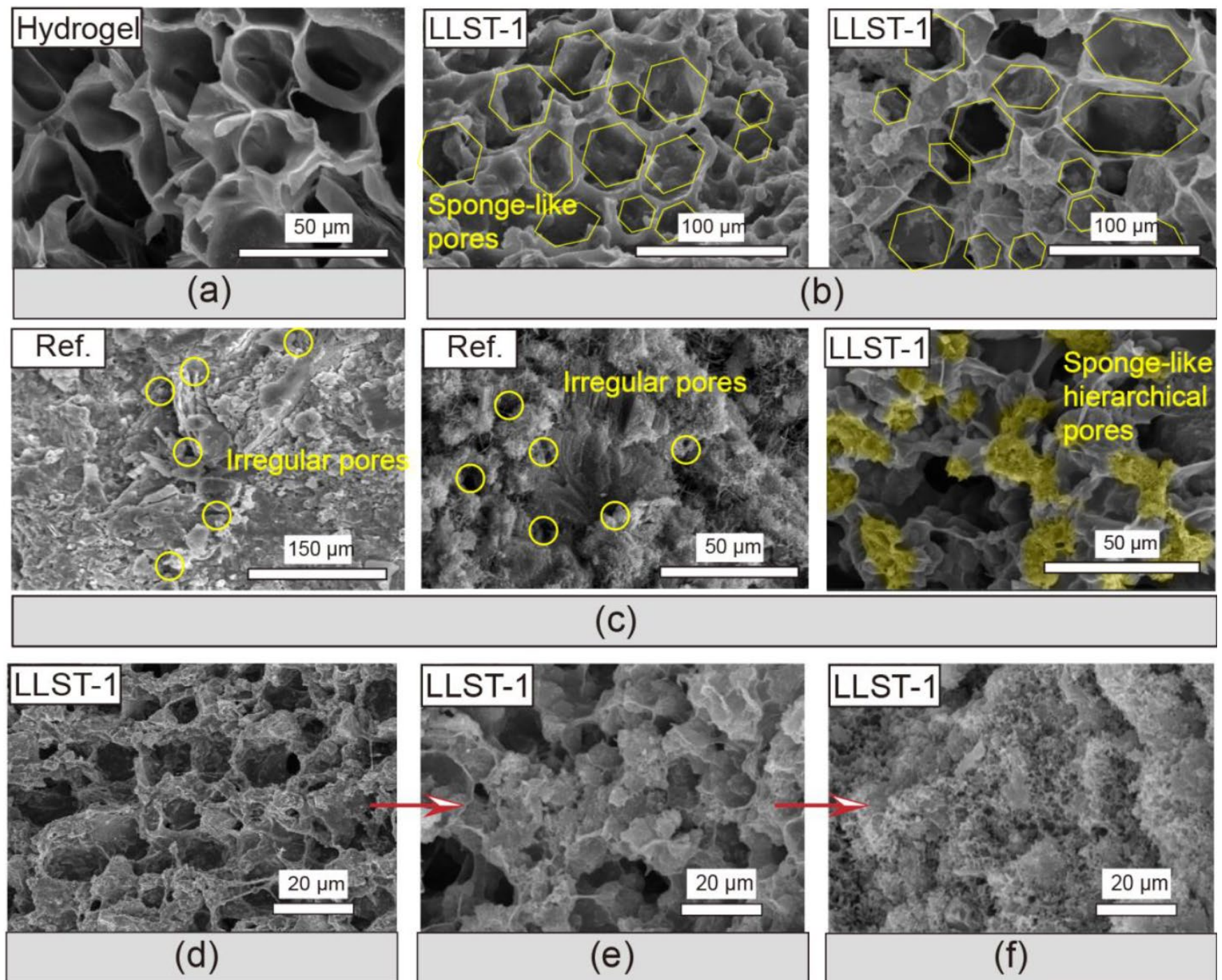
Microstructure of LLST

Fig. S.1.
(a) Pure hydrogel.
(b-c) Sponge-like pores in LLST.
(c) Pore shape in Ref. (irregular) and LLST (Sponge-like hierarchical pores)
(d-f) Microstructure of LLST after 10 min of fabrication, 7 and 28 days of hydration, respectively.
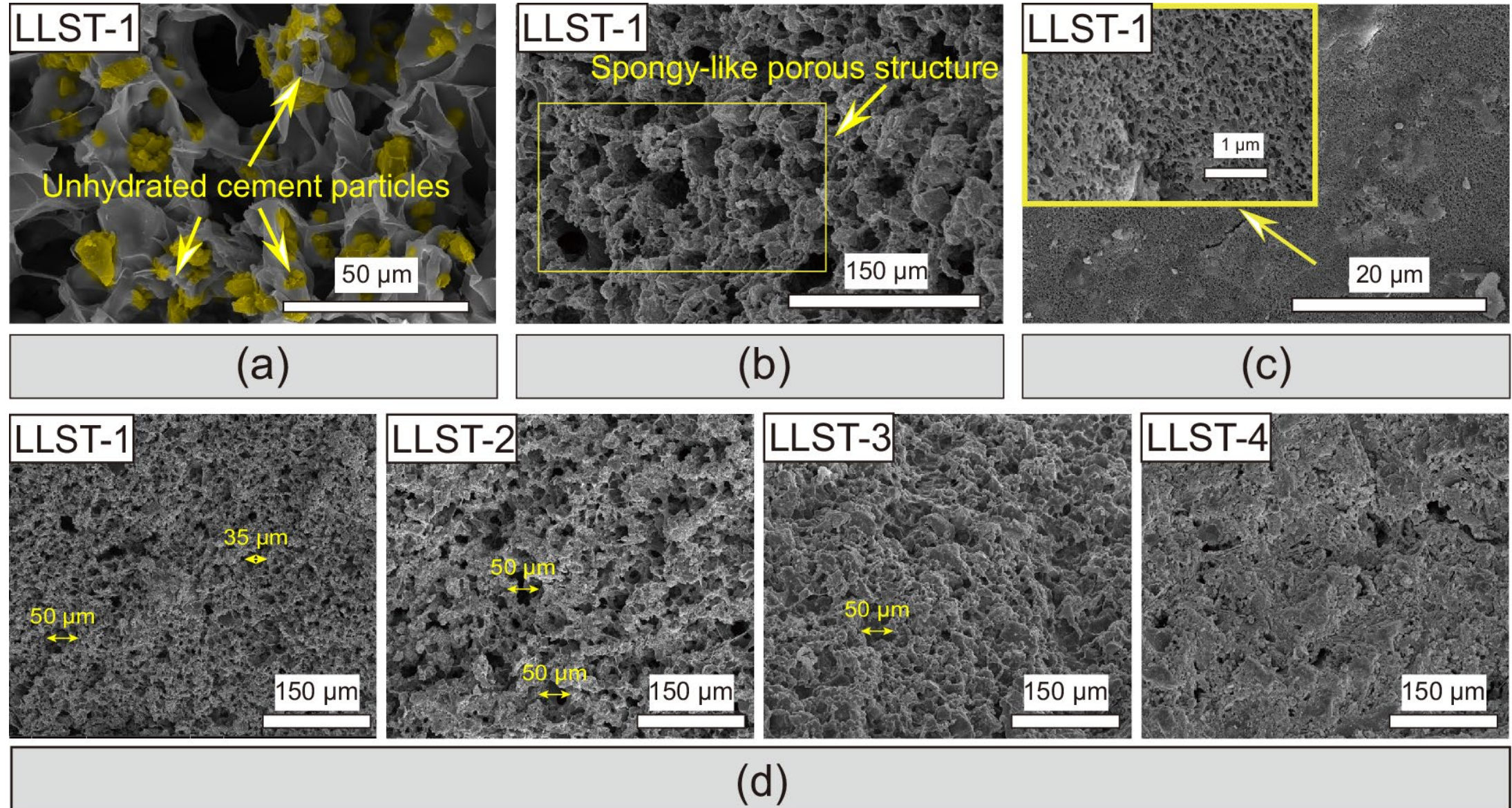
Microstructure of LLST

Fig.1. **(a)** The microstructure of LLST after 10 min of fabrication **(b)** The microstructure of LLST after 7 days of curing. **(c, d)** The microstructure of LLST after 28 days of curing. LLST-1, LLST-2, LLST-3, and LLST-4 corresponded to LLST with water to cement ratio (w/c) of 2, 1, 0.67, and 0.5.

Pore structure of LLST

1-50 μm micropores dominated in LLST-1

A significantly higher volume of 5 - 100 nm nanopores was present in all LLST.

Fig. 2 **(a)** Spatial distribution of micropores in LLST-1 obtained by **X-ray Computed Tomography (X-CT)**, where different pore sizes were labelled with different colours.
(b, c) Size distribution and cumulative volume of nanopores detected by **Mercury intrusion porosimetry (MIP).**
(d) Schematic hierarchical micro/nano porous structure.
LLST-1, LLST-2, LLST-3, and LLST-4 corresponded to LLST with w/c of 2, 1, 0.67, and 0.5, respectively. Ref. represented pure cement with a w/c ratio of 0.5.
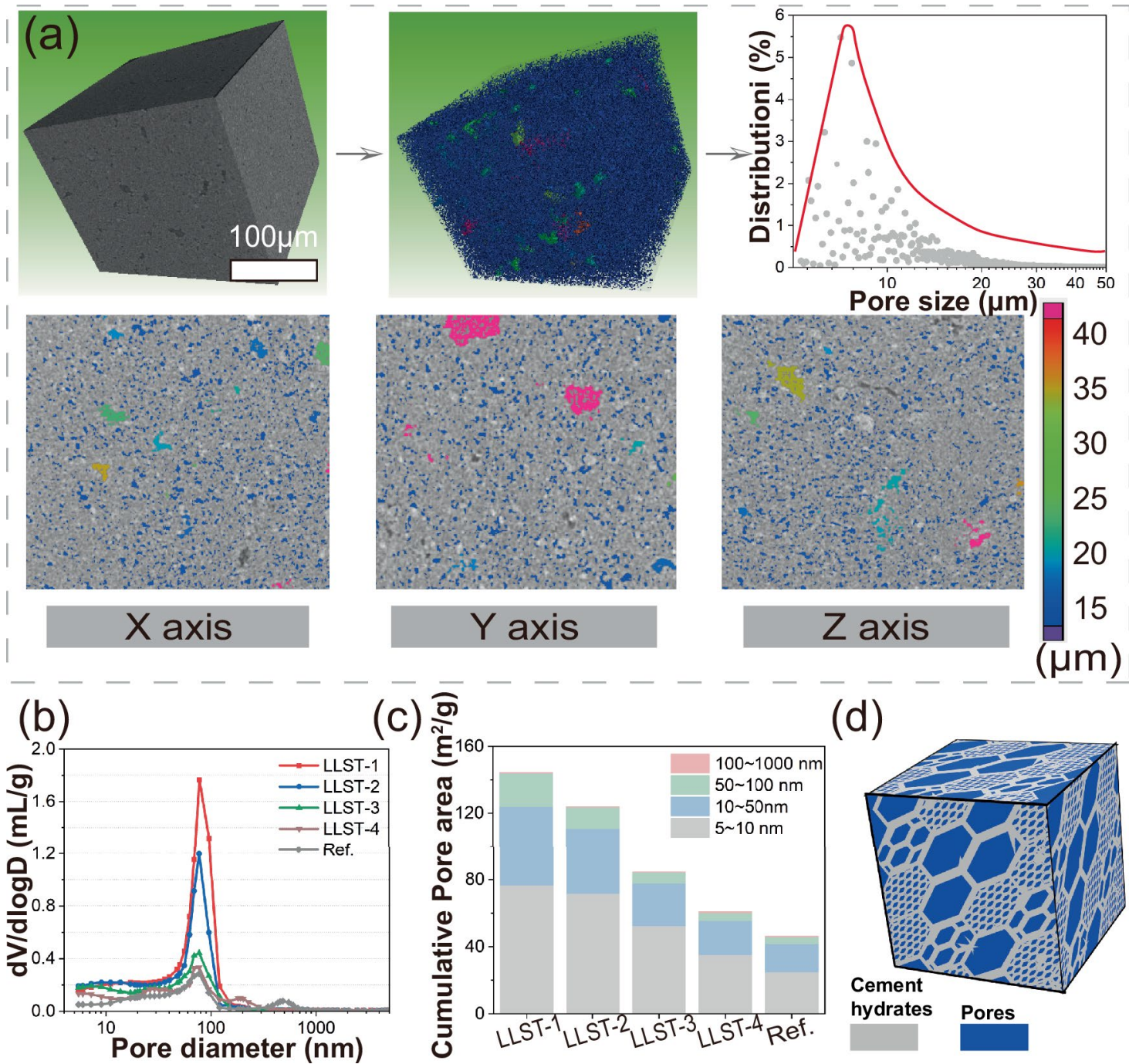
Mechanical properties

- **Compressive Stress:** The internal resistive force per unit area generated within a material when subjected to a compressive load. It causes volume reduction or shortening.

- **Specific Compressive Strength:** Compressive strength normalised by material density, indicating strength-to-weight efficiency.

- **Flexural Strength (Modulus of Rupture):** Maximum stress a material withstands under bending before fracture.

- **Midspan Deformation Rate:** Rate of vertical displacement at the centre of a beam during flexural testing, indicating toughness and ductility.
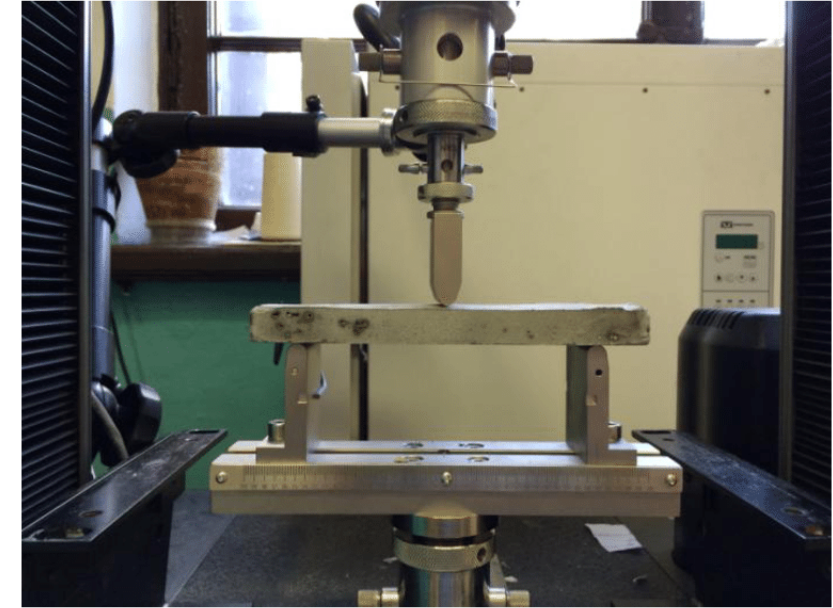
The specimen is oven drying at 40 °C for 24 h to remove water before mechanical strength testing.

Mechanical strength	Size of the specimen	Loading rate
Compressive test	20 mm cube	5 mm/min
Flexural test	20 × 20 × 80 mm cuboid	1 mm/min
Midspan deformation	20 × 20 × 80 mm cuboid	0.02 mm/min

Image credit: Google

Mechanical properties of LLST

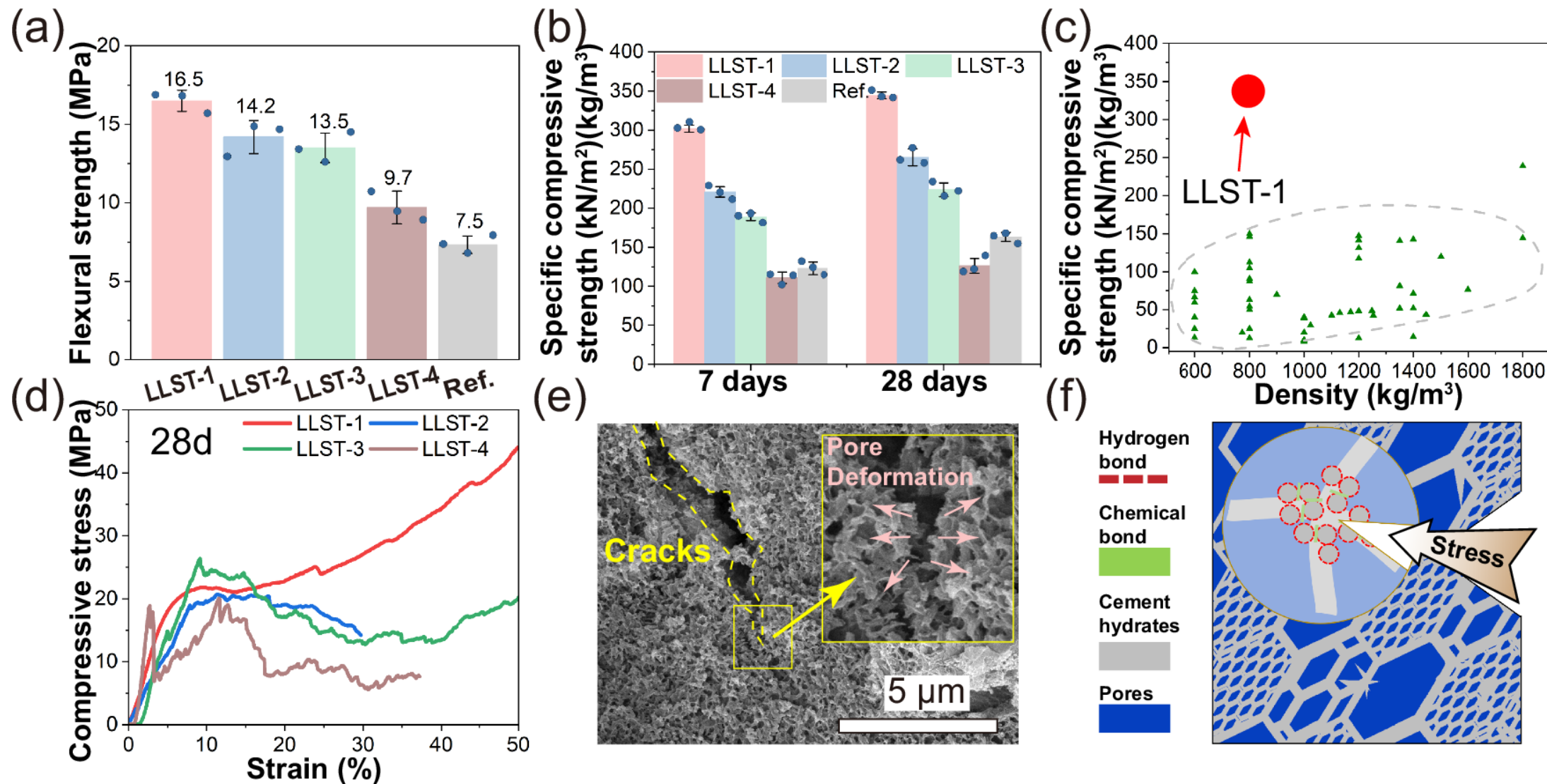Fig 3. (a) Flexural strength of LLST after 28 days of curing. The error bars in a, b represented the standard deviation, calculated based on three replicate experiments. (b) Specific compressive strength and (c) comparison with reported foam cement. (d) Strain-compressive stress curve of LLST. (e) Crack propagation was inhibited by pore deformation. (f) Schematic diagram of multi-scale stress dispersion.
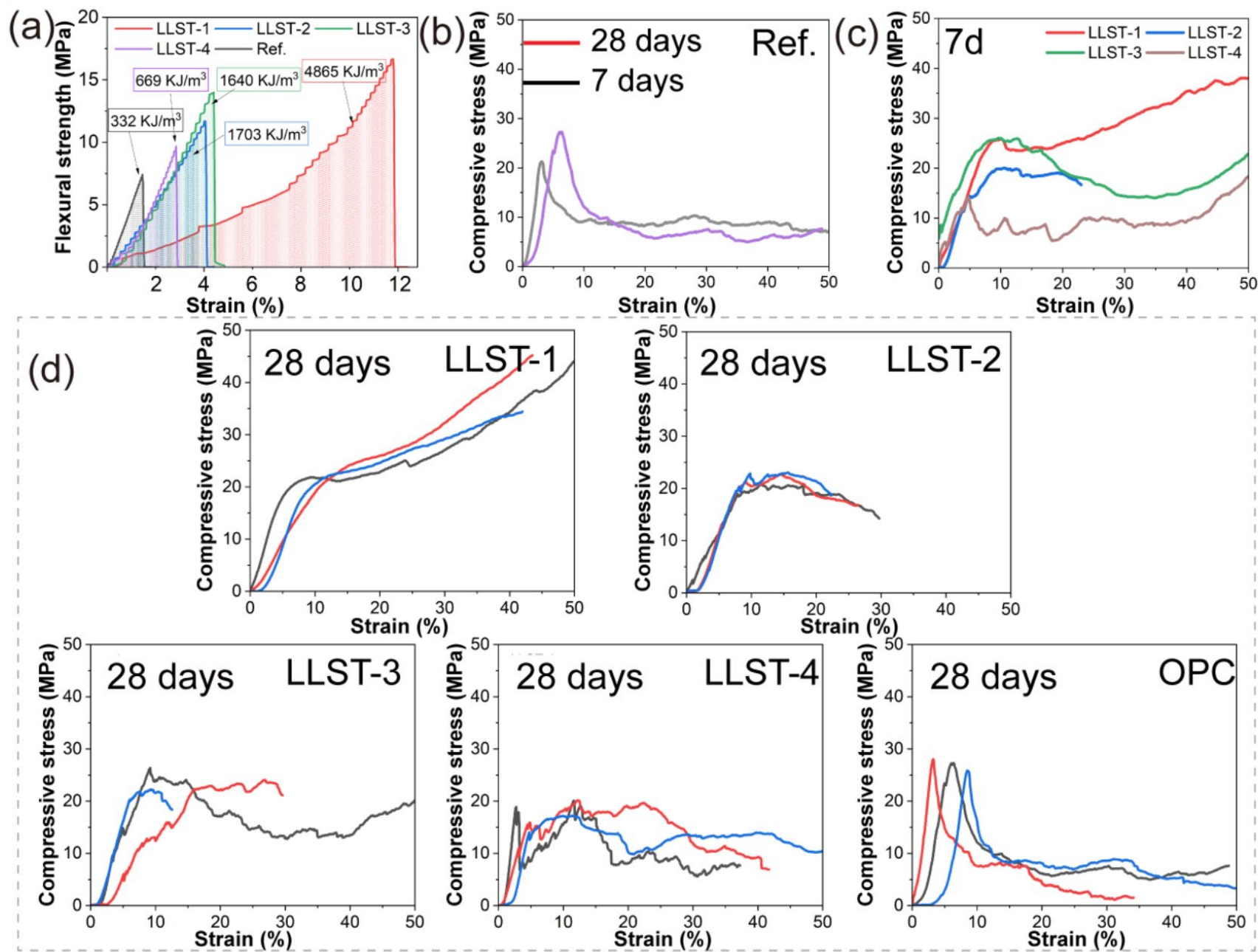
Mechanical properties of LLST

Fig. S. 3. **(a)** Midspan deformation rate and fracture energy of LLST at 28 days. **(b-c)** Load-displacement curve of Ref., and LLST. **(d)** Strain-compressive stress curve of LLST and OPC.

Fracture toughness (KIC)

$$K_{IC} = \frac{P_Q S}{BW^{3/2}} \left[2.9 \left(\frac{a}{W} \right)^{1/2} - 4.6 \left(\frac{a}{W} \right)^{3/2} + 21.8 \left(\frac{a}{W} \right)^{5/2} - 37.6 \left(\frac{a}{W} \right)^{7/2} + 38.7 \left(\frac{a}{W} \right)^{9/2} \right]$$

S-Table 1. Fracture toughness of LLST.

Specimen	a/W	f(a/W)	Pmax (N)	KIC (MPa·m$^{1/2}$)	Average (MPa·m$^{1/2}$)	Improvement (%)
	0.491	2.589	212.000	0.631		
LLST1	0.497	2.639	204.000	0.619	0.609	119.9
	0.486	2.549	197.000	0.577		
	0.493	2.606	194.000	0.581		
LLST2	0.499	2.656	185.000	0.565	0.561	102.5
	0.497	2.639	177.000	0.537		
	0.504	2.700	178.000	0.552		
LLST3	0.496	2.631	165.000	0.499	0.518	87.0
	0.489	2.573	170.000	0.503		
	0.495	2.623	110.000	0.331		
LLST4	0.498	2.648	144.000	0.438	0.398	43.7
	0.506	2.717	136.000	0.425		
	0.496	2.631	110.000	0.333		
Ref.	0.498	2.648	87.000	0.265	0.277	-
	0.492	2.598	78.000	0.233		

- P_Q represented the peak load from the load-displacement curve
- S is related to the span
- B is related to the width
- W is related to the height of the specimen
- a represented the notch depth.

Hydration characteristics of LLST

Fig. 4 **(a)** X-ray diffraction (XRD) pattern of cement hydrates in LLST and Ref. after 28 days of curing. CH, C_2S, C_3S, AFt, AFm corresponded to **calcium hydroxide, dicalcium silicate, tricalcium silicate, ettringite and monosulfoaluminate,** respectively. **(b–d)** Morphology of cement hydrates after 28 days of curing. **(e)** Hydration heat evolution within 7 days curing. **(f)** Hydration degree of LLST. Each sample was tested once. **(g–i)** Fourier Transform Infrared Spectrometer (FT-IR) spectra of Ref. and LLST after 7 and 28 days of curing.
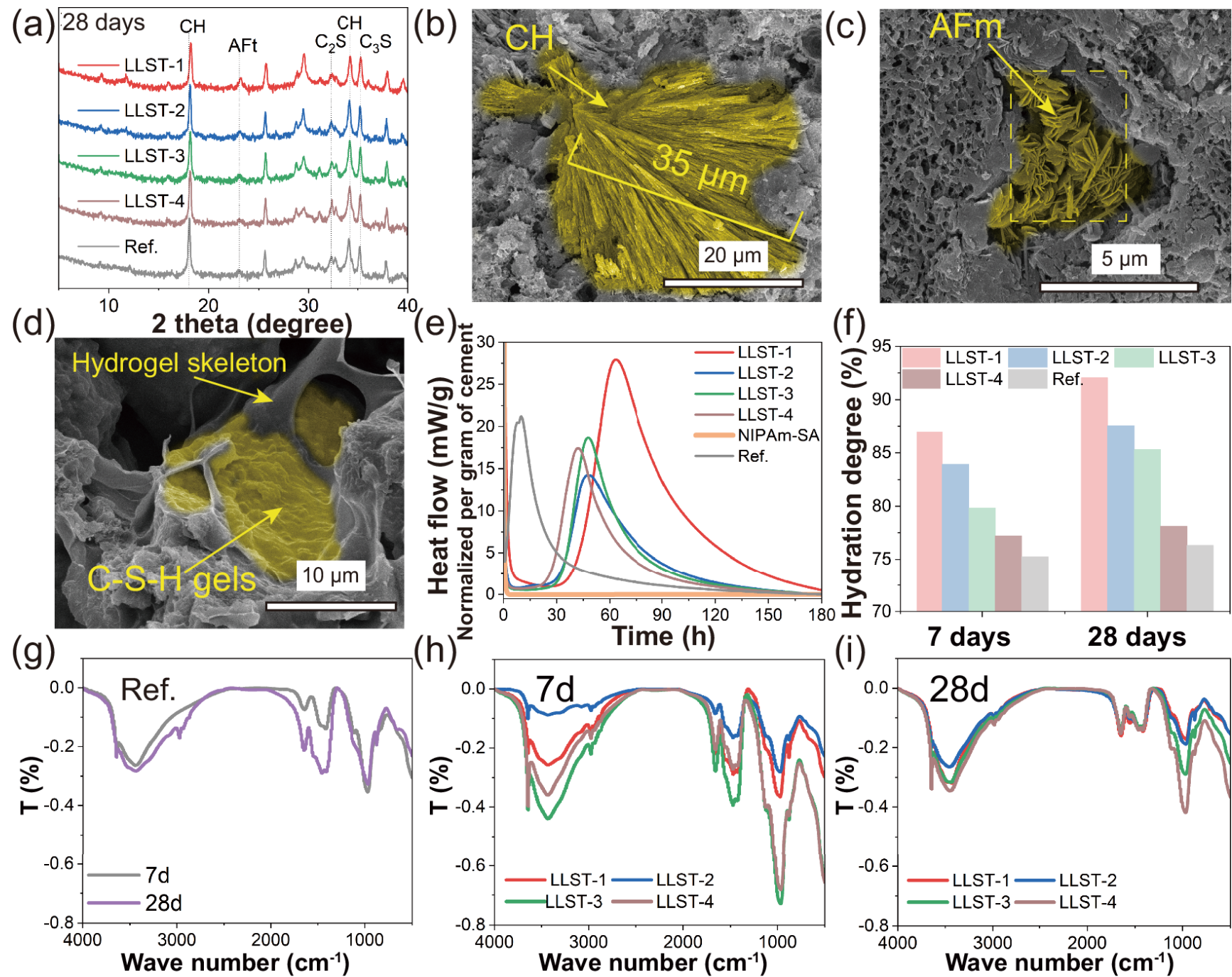
Molecular interaction mechanisms between the carboxyl group from hydrogel and the Ca ion released by cement particles
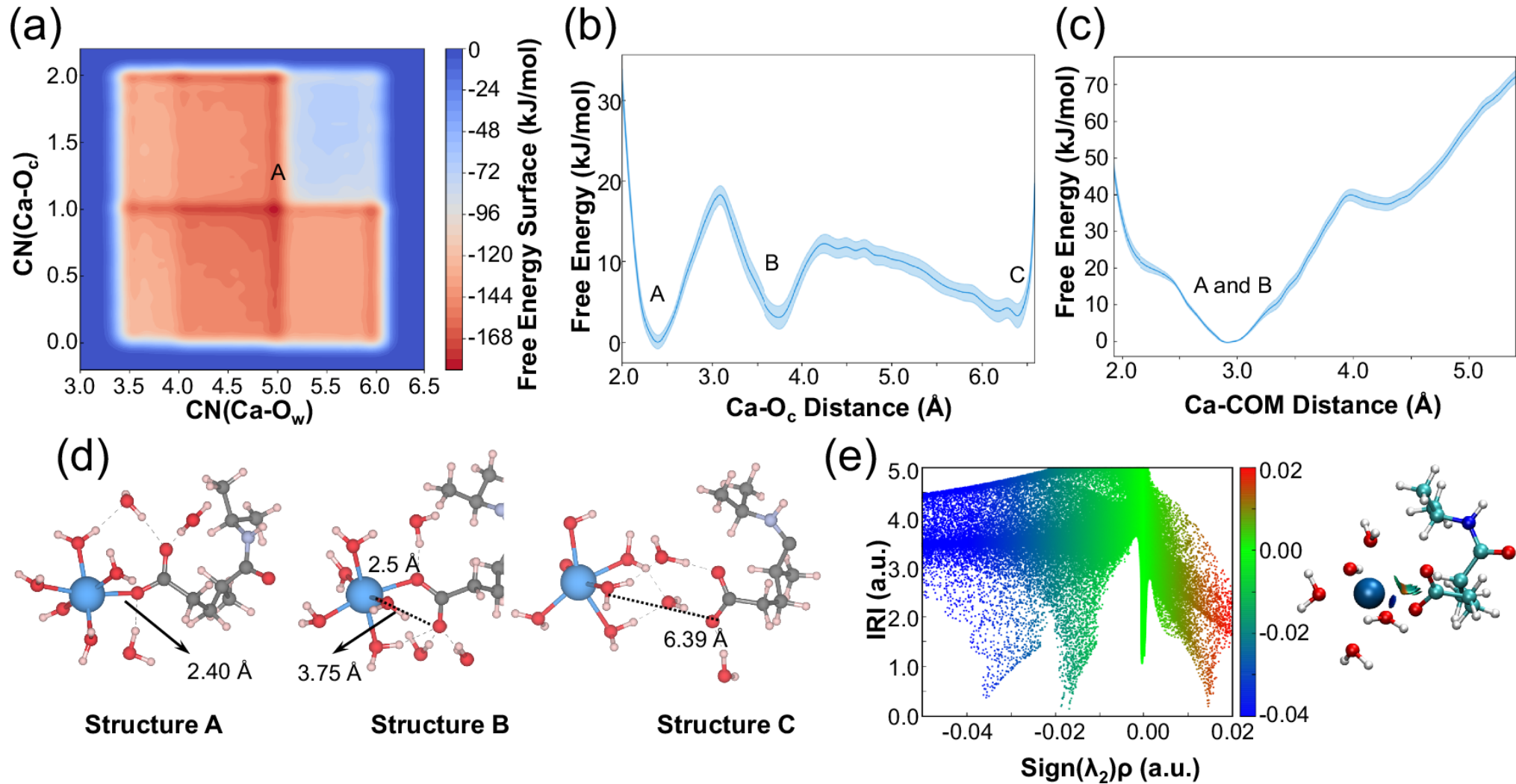

Fig 5. **(a)** Free energy profile with respect to the coordination number of the Ca ion with the O ion from the water (CN(Ca-Ow)) and the coordination number of the Ca ion with the O ion from the carboxyl group (CN(Ca-Oc)). **(b)** Free energy profile with respect to the distance between the Ca ion and one of the Oc ions. **(c)** Free energy profile with respect to the distance between the Ca ion and center of mass (COM) of two Oc ions. The shaded regions in (b and c) show the errors calculated by block analyses. **(d)** Configurations of the free energy minimum states on the FES. The blue, black, light purple, red, and white spheres are indicted to the calcium, carbon, nitrogen, oxygen and hydrogen. **(e)** Scatter map between sign(λ_2)ρ and IRI and isosurface map of IRI. Indigo, cyan, blue, red, and white spheres are indicted to the calcium, carbon, nitrogen, oxygen and hydrogen
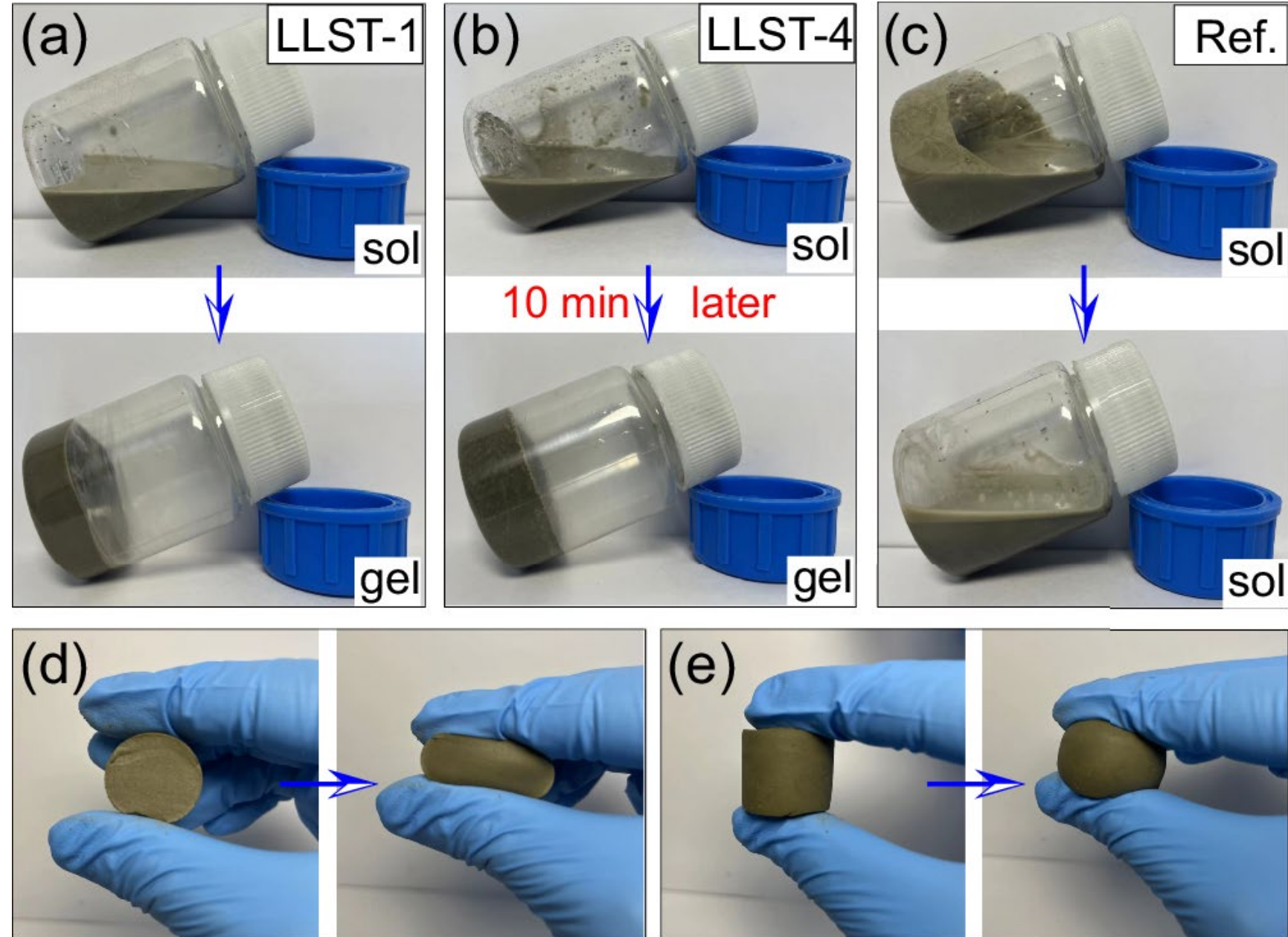
Gelation and elastic behavior of LLST

Fig 7. **(a–c)** After 10 min of mixing, LLST-1 and LLST-4 transitioned from a liquid to a solid state, whereas the Ref. group remained in the liquid state. **(d, e)** The elastic behaviour of LLST after gelation.

Conclusion

1. Hierarchical pore structure created using hydrogel templates: **micropores** (1–50 µm) and **nanopores** (5–100 nm), eliminating stress-concentrating macropores.

2. Performance improvements:

   - 54% lower density - **L**

   - 49% lower carbon emissions - **L**

   - 145% higher specific compressive strength - **S**

   - 1,365% increased fracture energy compared to traditional cement - **T**

3. Multi-scale **stress dispersion** via hierarchical pores and bonds (covalent, ionic, hydrogen) prevents crack propagation.

4. Hydrogel transforms water supply **from free water to confined water**, ensuring uniform hydration and better material compatibility.

5. Strong **chemical bonding** (Ca^{2+}–O from carboxyl groups) confirmed by **simulations**, enhancing structural stability.

6. Fabrication involves rapid hydrogel gelation (**10 minutes**) and cement hydrate deposition, enabling scalable production.